Quantum Control of Molecular Wavepackets: An Approximate Analytic Solution for the Strong-Response Regime

Luís E. E. de Araujo* and Ian A. Walmsley

The Institute of Optics, University of Rochester Rochester, New York 14627

Received: July 12, 1999; In Final Form: September 9, 1999

We derive a simple approximate analytic solution for the driving field that will generate a desired target vibrational wavepacket in a diatomic molecule. This solution is valid for arbitrary population transfer from the initial to the final electronic states. Analytic solutions to the control problem are possible when the control field is of shorter duration than the characteristic time scale of the system being manipulated. For target states that are localized wavepackets, our technique yields multiple solutions for the control field. We describe a procedure to choose from the set of solutions one that achieves both the target state and population transfer with high accuracy, for a large class of target states. The fidelity of each solution is tested by comparing the state obtained from a direct numerical integration of Schrödinger's equation using the analytic solution with the specified target state.

I. Introduction

The manipulation of fundamental constituents of matter at their most basic level has long been an important goal of many branches of science. In the recent past, several experiments have shown that it is possible to create chosen quantum states of atoms[1,2] and molecules,[3−7] and to characterize them completely.[8−11]

These experiments are in some ways the culmination of a decade's research into the central problem of quantum control. Two approaches have been suggested to quantum control: coherent radiative control,[12,13] in which two or more cw fields are used to interfere different pathways to the final target state; and optimal control,[14−19] which searches for the optimal pulses that best steers the system to the chosen target state. These two schemes have been successfully implemented, for example, in controlling molecular dissociation,[20−23] carrier dynamics in semiconductors,[24−26] product ratio in chemical reactions,[6,27−29] state-selective vibrational excitation of molecules,[30−32] and wavepacket dynamics in the gas[5,33−38] and condensed phases.[39,40]

In optimal control theory (OCT), a cost functional is postulated and the shape of the field is varied to maximize this functional. This functional contains information about the target, which may be the state of the system, and relevant penalties or physical constraints, such as the requirement of a finite pulse energy. This procedure usually leads to a set of highly nonlinear coupled partial differential equations. These equations must be solved iteratively, starting from an initial guess for the driving field, until eventually the field converges to a solution after a number of iterations. In the weak-response regime, it is possible to find analytic solutions for the driving field from these equations.[41] The nonlinear strong-response regime, when significant population transfer from the initial to the final state is specified, has only been dealt with numerically.[34,37,42]

Despite the success of OCT in predicting control fields, numerical methods usually tend to obscure the physics of the problem. For example, it is usually very hard even to just understand why the control fields, obtained with OCT, have the shape they do. This motivates us to seek an analytic solution to the control problem in the strong-response regime. Such a solution is important for developing an understanding of the physics in the strong-response regime of excitation, and in particular to deconstruct the final shape of the control field. Also, as recently pointed out by Zhu and Rabitz,[43] in some cases only a good estimate for the control field is necessary. These may be used, for example, as inputs to learning procedures that are implemented experimentally. Zhu and Rabitz describe a general noninterative algorithm which yields an approximate semianalytic solution for the control field; evaluation of the control field depends on the numerical solution of Schrödinger's equation for the wave function.

An alternative approach to solving the control problem involves solving Schrödinger's equation analytically in a regime that takes advantage of some of the known physical dynamics of the situation. Recently, we derived an approximate analytic expression for the driving field that generates a specified radial wavepacket in Rydberg atoms.[44] We showed that by imposing the duration of the excitation pulse to be shorter than a Kepler period, the driving field so determined works extremely well for arbitrary population transfer to the Rydberg series.

In this article, we extend that method to the case of diatomic molecules. We show that a similar approximate analytic solution can be found for the field that will generate an arbitrary vibrational wave packet in homonuclear diatomic molecules. As we will show, this approximate control field is evaluated directly from the target probability amplitudes, and it holds well even in the strong-response regime. The feature of molecules that is different from atoms, so far as this problem is concerned, is that the ground electronic state is itself a manifold: there are many vibrational levels in each electronic state. Population can be trapped in these vibrational levels via Raman-like transitions, limiting the amount of population that can be transferred from the ground to an excited electronic state. The key to obtaining a good solution is to choose among the many possible solutions one that is long enough to avoid such population trapping, and

* Corresponding author. E-mail: walmsley@optics.rochester.edu.

10.1021/jp992323r CCC: $18.00
Published on Web 11/19/1999

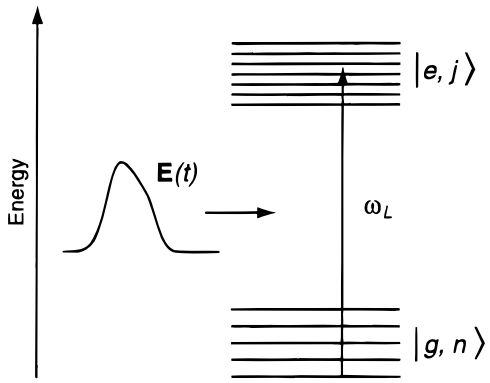

Figure 1. Model system to be controlled. The states within the ground manifold, g, are labeled by the quantum number n; and states within the excited manifold, e, are labeled by the quantum number j. The sought electric field $\mathbf{E}(t)$ is assumed to be resonant with a $g \rightarrow e$ transition.

yet, that is still short enough that the discreteness of the system's level structure is not operative.

Even though we will discuss the technique with respect to a diatomic molecule, it could in principle be extended to a variety of systems consisting of a ground and an excited manifold of states, of the type shown schematically in Figure 1. Many quantum systems have at least part of their structure of this type: the internal degrees of freedom of atoms and molecules, interband transitions in quantum-confined semiconductors, the center of mass of motion of trapped ions and atoms, to name a few. It is a simple matter to determine if the system is controllable, using our method, once its spectrum and coupling matrix are known. The spectrum may represent the states corresponding to several degrees of freedom of the optically excited particle, and to that extent, some control should be possible for multidimensional systems. In any case, it is possible to determine from this information what range of the Hilbert space of the system may be accessed using this technique.

This paper is organized as follows: in section II, we derive the differential equations governing the time evolution of the probability amplitudes of the vibrational-electronic states; in section III, we discuss population trapping in the ground state and how it can be avoided; we derive an analytic solution for the driving field in section IV; we present the numerical results in section V; and finally, we conclude by discussing the possible applications of this method in section VI.

II. Time Evolution of the Probability Amplitudes

The sort of systems we are trying to control has an energy level structure of the kind shown in Figure 1. Each energy level within the upper (excited) manifold is connected to the levels in the lower (ground) manifold by time-dependent interaction, but no direct interaction is allowed between different levels within each manifold. In the case of a diatomic molecule driven by an external optical field, $\mathbf{E}(t)$, the two manifolds correspond to molecular vibrational−electronic states connected by dipole transitions.

The goal is to find the electric field that will create a target wavepacket, centered at $j = \bar{\nu}$, in the excited manifold starting from an initial state in the ground manifold.

We start by writing the state of the system at some arbitrary time t in terms of the unperturbed eigenstates of the molecule: $|\Psi\rangle = \sum_{n=0}^{N} a_n(t) e^{-i\omega_{gn}(t-t_0)} |g,n\rangle + \sum_{j=0}^{M} b_j(t) e^{-i\omega_{ej}(t-t_0)} |e,j\rangle$, where $|g,n\rangle$ and $|e,j\rangle$ are the ground and excited vibrational−electronic states, respectively; N and M are the number of vibrational eigenstates supported by each of the potentials; and ω_{g0}, the eigenfrequency of state $|g,0\rangle$, is defined to be equal to zero. We assume for $t \le t_0$ that $b_j(t) = 0$, and $a_n(t) = \delta_{n0}$. That is, all the population is initially in the ground vibrational-electronic state. The equations governing the time evolution of the probability amplitudes $a_n(t)$ and $b_j(t)$ are then found directly from Schrödinger's equation: $(i\hbar)\partial|\Psi\rangle/\partial t = \hat{H}|\Psi\rangle$.

The simple two-manifold model of Figure 1 applies to the excitation of an electronic−vibrational transition in a molecule, if rotations are ignored. The Hamiltonian describing the interaction of the diatomic molecule with the external classical field $\mathbf{E}(t)$ can be written as

$$\hat{H} = \hbar\left(\sum_{n=0}^{N} \omega_{gn} |g,n\rangle\langle n,g| + \sum_{j=0}^{M} \omega_{ej} |e,j\rangle\langle j,e|\right) - \hat{\mathbf{d}}\cdot\mathbf{E}(t) \quad (1)$$

In the above equation, the first term in the right-hand side (RHS) corresponds to the bare adiabatic Hamiltonian that governs the field-free evolution of the system. The second term is the interaction Hamiltonian, corresponding to dipole transitions excited by the electric field. Such a Hamiltonian model for wavepacket excitation is very common in the literature.[34,38,45]

The electric field, linearly polarized along the dipole moment $\hat{\mathbf{d}}$, is written as $\mathbf{E}(t) = E_0[f(t)e^{-i\omega_L(t-t_0)} + \text{c.c.}]$. With $f(t) \equiv |f(t)|e^{i\phi(t)}$, then $|f(t)|$ is the dimensionless slowly-varying amplitude of the field, $\phi(t)$ is its phase, and ω_L is the carrier frequency. We take $\omega_L = \omega_{e\bar{\nu}}$, and $E_0 = 1$ V/m. Except for the constraint $f(t \le t_0) \equiv 0$, the form of $f(t)$ is not prescribed initially.

Applying the rotating wave approximation, we then find a set of coupled differential equations for the probability amplitudes:

$$\dot{a}_n = if^*(t) \sum_{j=0}^{M} \Omega_{nj} b_j(t) e^{-i(\delta_j - \omega_{gn})(t-t_0)} \quad (2)$$

$$\dot{b}_j = if(t) \sum_{n=0}^{N} \Omega_{nj}^* a_n(t) e^{i(\delta_j - \omega_{gn})(t-t_0)} \quad (3)$$

where $\Omega_{nj} \equiv \langle n,g|\hat{d}|e,j\rangle E_0/\hbar$, and $\delta_j = \omega_{ej} - \omega_L$ is the detuning for each transition.

Substitution of the formal integration of eq 3 into eq 2 gives

$$\dot{a}_n = -\Omega_{n\bar{\nu}} e^{i\omega_{gn}(t-t_0)} f^*(t) \int_{t_0}^{t} ds\, f(s) \sum_{m=0}^{N} \Omega_{m\bar{\nu}}^* e^{-i\omega_{gm}(s-t_0)} \times a_m(s)\xi_{nm}(t-s) \quad (4)$$

Here, $\xi_{nm}(t-s) \equiv \sum_{j=0}^{M} (\Omega_{nj}\Omega_{mj}^*/\Omega_{n\bar{\nu}}\Omega_{m\bar{\nu}}^*) e^{-i\delta_j(t-s)}$ is an electronic "response" function for the transition $|g,n\rangle \rightarrow |e,j\rangle$. It can be seen that the response function is an anharmonic series whose terms have an amplitude proportional to the Franck−Condon factors connecting pairs of levels in the ground state via transitions to the upper state. For n and $m = 0$, the response function $\xi_{00}(t-s)$ consists of a series of impulses of decreasing amplitude and increasing duration, centered at approximately $s \approx t - k\mathrm{T}$ (with $k = 0, \pm1, \pm2, \ldots$; and $\mathrm{T} = 1/\nu_e \equiv 2\pi/(\omega_{e1} - \omega_{e0})$ being the vibrational period of the excited electronic state). It is a general characteristic of such series that they have a maximum at $s = t$, whose width decreases as the number of terms in the series increases. Figure 2 shows a graph of a typical function $\xi_{00}(t-s)$, in this case, for the iodine molecule. It has a strong narrow peak centered at $s = t$, smaller and longer peaks at $s \approx t \pm 2\mathrm{T}$, and small short-period oscillations everywhere else.

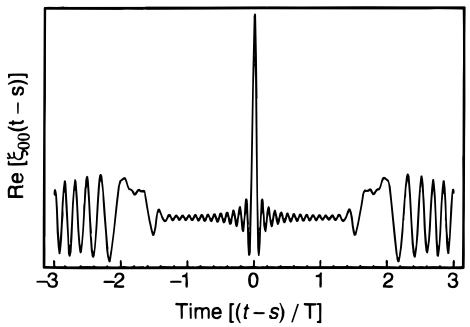

Figure 2. Electronic "response" function $\xi_{00}(t - s)$ for the B state of I_2. $M = 55$ states were included in the sum.

If $h(t)$ is an arbitrary function with compact support between $0 \le t - t_0 \le T$ (that is, $h(t)$ is nonzero only inside this interval), then to a good approximation

$$\int_{-\infty}^{t} ds\, h(s)\xi_{00}(t - s) \approx \frac{1}{2}(\eta_0/\nu_e)h(t) \tag{5}$$

where $\eta_0 = \nu_e \int_{-T/2}^{T/2} ds\ \xi_{00}(s)$. An important requirement on $h(t)$ for eq 5 to hold is that it should not have any structure that is short in duration compared to the response function $\xi_{00}(t)$. In this case, the small oscillations seen in Figure 2 average out to zero when performing the integration in eq 5. The center impulse in Figure 2 is the important feature of $\xi_{00}(t)$ here: it picks out the value of $h(s)$ at $s = t$. To a very good approximation, the electronic response function behaves like Dirac's delta function. In the case of a harmonic manifold, the various δ_j are evenly spaced, and $\eta_0/\nu_e \approx 1$ because the response function $\xi_{00}(t)$ resembles very closely a series of evenly spaced delta functions (this result is known as the Poisson sum formula[46]). Depending on the anharmonicity of the excited electronic state, the requirement that $h(t)$ be restricted to one vibrational period can be considerably relaxed (e.g., as for the iodine molecule).

However, for $n, m \neq 0$, $\xi_{nm}(t - s)$ does not in general exhibit the same features seen in $\xi_{00}(t - s)$. The generalization of eq 5 for arbitrary n, m is an approximation that must be checked for each system.

The complexity of the eigenstate spectrum will clearly determine whether the time scales of the electronic response function are appropriate for determining the control field analytically. The general requirements are that a large number of states in the excited manifold be accessible from each state in the ground manifold and that the coupling matrix elements should vary slowly as a function of n and m.

III. Ground State Depletion and Population Trapping

The short response-function approximation could be used to greatly simplify eq 4 if, throughout the excitation, the population remained in the ground state, that is, $a_{m\neq 0}(t) \approx 0$. However, due to the large bandwidth of the short driving pulses, population may be transferred back down from the excited state to the other ground vibrational levels via impulsive stimulated Raman scattering.[47,48] Population returns to the lower states with just the right phase so that further ground state depletion is inhibited, and is then trapped in the ground electronic state. A similar problem arises in the ionization of Rydberg atoms.[49,50]

Such Raman-like transitions were studied in some detail by Dubrovskii et al.[50] who derived conditions on the pulse duration and profile under which population trapping could be avoided when ionizing a Rydberg atom. Generally speaking, population trapping occurs when the driving field is switched on too fast, quickly going from the weak-response to the strong-response regime. In the weak-response regime, the initial Rydberg level experiences an increasing rate of ionization with increasing intensity, while in the strong-response regime, this rate tends to decrease with intensity. At the boundary of the two regimes, the decay rate goes through a maximum. Population trapping is avoided by slowly turning the pulse on so that the pulse spends more time around that point of maximum ionization. When the pulse goes into the strong-response regime, and population trapping begins to dominate, most population has already been ionized to the continuum.

A similar result for strong-response excitation of molecules appears in quite a different context. Cao et al.[51] showed that by chirping a pulse, a molecular "π pulse" could be designed, leading to an almost complete population inversion between two electronic states of a diatomic molecule. They also observed that shorter pulses failed to accomplish such an inversion, with population remaining trapped in the ground electronic state after excitation. Their explanation of this phenomenon centered on a wavepacket picture of the excitation dynamics. The similarity between ionization of Rydberg atoms and excitation of molecules comes from the fact that the excited localized state of the molecule takes at least one vibrational period to "notice" the discreteness of the excited state. Up to this point, the excited manifold looks just like a continuum and the molecular dynamics of dissociation and vibration remains identical.

Considering both arguments, we postulate that if the driving field is long enough to avoid trapping in the lower manifold, but still shorter than one vibrational period, ground-vibrational levels other than $m = 0$ will remain unpopulated throughout excitation. This approximation must, of course, be checked after the fact, but this is a simple forward integration of Schrödinger's equation. In deriving an analytic solution, we take $a_{m\neq 0} \approx 0$ in eq 4. Then, using eq 5, we arrive at

$$a_n(t) \approx \begin{cases} \exp[-\eta_0 G(t)], & \text{if } n = 0 \\ 0, & \text{if } n \neq 0 \end{cases} \tag{6}$$

where

$$G(t) \equiv (1/2)(\nu_e |R_0|^2)\int_{t_0}^{t} |f(t)|^2\, ds \tag{7}$$

is proportional to the pulse energy up to time t. Here, $R_0 \equiv \Omega_{0\bar{v}}/\nu_e$.

Note that no assumption about the shape of $f(t)$ has been made. We assume only that the driving pulse is long enough to avoid population trapping, but no particular value is assigned to its duration. Because the exact shape of $f(t)$ depends on the target wavepacket (not yet specified), an estimate (such as the ones derived by Dubrosvkii[50]) on how long the driving pulse has to be in order for eq 6 to hold cannot be made at this point. If the driving field turns out to be so short that eq 6 is not a good approximation, that will be reflected on the field's inability to drive the system toward the target state with good fidelity.

It is important to point out that in arriving at this result, no approximation was made regarding the strength of the field beyond the constraint that the field should not be so strong that the ground state is depleted significantly during the duration of the electronic response function $\xi_{00}(t-s)$ (and of course, that the two-manifold model itself remains valid at all times). Nonetheless, we do allow the ground state to deplete over the duration of the control pulse itself. This is in fact how we define strong-response excitation. Equation 6 indicates that no Rabi cycling of the population between the ground and excited states can occur during the first vibrational period. This is because quantum interference suppresses the transfer of population from

the "bright" state, created in the excited manifold, back to the ground state. In a wavepacket picture, the localized state that is excited by the pulse does not complete an entire period of oscillation during the time that the driving field is nonzero; there is no possibility that the end of the driving pulse can cycle population from the initially excited part of the wavepacket back to the ground state.

The requirement of a pulse width shorter than the vibrational period means the excitation is nonadiabatic. The process we describe is in the regime of quasi-impulsive excitation, and not at all in the regime of adiabatic following.[51]

IV. Driving Field

In the weak-response limit, since the population in the ground electronic state does not change appreciably during excitation, the driving field can be found easily by directly integrating eq 3 and then taking its inverse Fourier transform. In the more general case of significant ground state population depletion, the driving field can still be found directly from the *given* set of target amplitudes $b_j^{(T)}$ (with $\sum_{j=0}^{M}|b_j^{(T)}|^2 = \Delta$, Δ being the target depletion) for the desired wavepacket at some target time τ, when the field is again zero.

Substitution of eq 6 back into eq 3 yields at the target time τ:

$$B(t) = i\Omega_{0\bar{\nu}}^{*}\int_{-\infty}^{\infty} \mathrm{d}s\, f(s)\mathrm{e}^{-\eta_0 G(s)}[\sum_{j=0}^{M}\mathrm{e}^{-i\delta_j(t-s)}] \qquad (8)$$

Here, we set $b_j(\tau) = b_j^{(T)}$ and defined $B(t) \equiv \sum_{j=0}^{M}(\Omega_{0\bar{\nu}}/\Omega_{0j})^* b_j^{(T)}\mathrm{e}^{-i\delta_j(t-t_0)}$. Because $f(t)$ is limited, by construction, to one vibrational period, the integration limits in eq 8 could be extended to $\pm\infty$.

As before, if a function $h(t)$ has compact support between 0 and T, then

$$\int_{-\infty}^{\infty} \mathrm{d}s\, h(s)\,[\sum_{j=0}^{M}\mathrm{e}^{-i\delta_j(t-s)}] \approx (\eta/\nu_e)h(t) \qquad (9)$$

where $\eta \equiv \nu_e\int_{-\mathrm{T}/2}^{\mathrm{T}/2} \mathrm{d}s\, \sum_{j=0}^{M} \mathrm{e}^{i\delta_j s}$.

Using the above approximation in eq 8 yields

$$f(t) = i(\eta R_0)^{-1}\mathrm{e}^{\eta_0 G(t)}\, B(t) \qquad (10)$$

At first glance, eq 10 looks like a transcedental equation for $f(t)$. Since $f(t)$ enters the RHS through $G(t)$, one might expect that this equation could only be solved numerically. However, it turns out that this is not the case. As we show next, we can solve for the dynamics of $G(t)$ first, and substitute it back into eq 10 to evaluate the field. Taking the derivative of $G(t)$ (defined in eq 7), we obtain the result $\dot{G}(t) = (1/2)(\nu_e|R_0|^2)|f(t)|^2$. Substituting eq 10 into this equation yields

$$\dot{G}(t) = [(\nu_e/2|\eta|^2)|B(t)|^2]\mathrm{e}^{(\eta_0^*+\eta_0)G(t)} \qquad (11)$$

It is straightforward to integrate eq 11 for $G(t)$, arriving at

$$\mathrm{e}^{-(\eta_0+\eta_0^*)G(t)} = 1 - [(\eta_0 + \eta_0^*)/2|\eta|^2]\nu_e\int_{t_0}^{t}|B(s)|^2\,\mathrm{d}s \qquad (12)$$

From eq 6, the ground state population at time t is $\sum_{n=0}^{N}|a_n(t)|^2 = \mathrm{e}^{-(\eta_0+\eta_0^*)G(t)}$. If we require population to be conserved at all times, so that $\sum_{n=0}^{N}|a_n(t)|^2 + \sum_{j=0}^{M}|b_j(t)|^2 = 1$ for all t, then at the target time τ, $\sum_{j=0}^{M}|b_j(\tau)|^2 = [(\eta_0 + \eta_0^*)/2|\eta|^2]\nu_e\int_{t_0}^{\tau}|B(s)|^2$ ds. Because of the Franck−Condon factors in the definition of $B(t)$ and the anharmonicity of the excited manifold, in general the excited state population $\sum_{j=0}^{M}|b_j(\tau)|^2$ will not be equal to Δ, the target depletion. The amplitudes $b_j(t)$ (and similarly, $a_n(t)$) need to be renormalized. We define $\chi = \Delta/\int_{t_0}^{\tau}|B(s)|^2$ ds so that $\sum_{j=0}^{M}|b_j(t)|^2 = \chi\int_{t_0}^{t}|B(s)|^2$ ds, and at $t = \tau$, the proper depletion is achieved. Equation 12 then becomes: $\exp[-(\eta_0 + \eta_0^*)G(t)] = 1 - \chi\int_{t_0}^{t}|B(s)|^2$ ds, which can then be substituted back into eq 10 to evaluate the field. Because this is an inverse problem, conservation of population is not automatically guaranteed when substituting eq 6 into eq 3: The RHS of eq 8 is not properly normalized with respect to the LHS, and population conservation must be introduced explicitly.

The field that generates the target distribution $b_j^{(T)}$ in the excited electronic state is then found to be

$$f(t) = i(\eta R_0)^{-1}\frac{B(t)}{(1 - \chi\int_{t_0}^{t}|B(s)|^2\,\mathrm{d}s)^{\eta_0/(\eta_0+\eta_0^*)}} \qquad (13)$$

From eq 13, $f(t)$ can be evaluated directly from the target amplitudes, thus completely determining the driving field $\mathbf{E}(t)$. In the case of molecules with weakly anharmonic electronic potentials, eq 13 can be simplified even further by observing that $\eta \approx \eta_0 \approx 1$.

Equation 13 is one of the major results of this paper and it represents a prescriptive solution for creating a target wavepacket in diatomic molecules, for arbitrary population transfer. If the target wavepacket is well localized, the function $B(t)$ consists of a series of impulses of decreasing amplitude that gradually broaden into one another. The more anharmonic the excited state is, the longer these impulses are, and the more they overlap. It is clear from the weak-response solution (obtained from eq 13 by letting $\chi \rightarrow 0$) that each of the isolated impulses contains a complete specification of the target wavepacket. In the weak-response regime, any of these impulses can be used in eq 13 to determine the driving field. However, in the strong-response regime, the only impulses that will work are the ones that yield a pulse that is long enough to avoid population trapping in the ground electronic state. Of course, these considerations restrict the set of possible target wavepackets to those for which $B(t)$ has this quasi-periodic structure. Because of the Ω_{0j}^{-1} factor in the definition of $B(t)$, these possible targets are those for which the probability amplitudes lie within the states accessible via a Franck−Condon transition from the initial vibrational−electronic state.

In practice, one chooses a particular impulse from $B(t)$ by choosing a value for t_0. Assigning a value to t_0 the moment the pulse switches on has no real physical meaning since in the laboratory there exists no absolute time origin. However, the choice of such an origin is implicit in the definition of the electronic response function $\xi_{00}(t)$ (and similarly in eq 9): the central peak of $\xi_{00}(t)$ is located at $t = 0$. Furthermore, eqs 5 and 9 assume the nonzero portion of the driving field to be located between 0 and T. Choosing a value for t_0 simply brings a particular impulse of $B(t)$ into this interval. Similarly, the value of τ is arbitrary. The physically meaningful quantity is the delay between the turn on of $f(t)$ and the target time: $\tau_0 \equiv \tau - t_0$. This is the time after the driving pulse has switched on that we expect the excited amplitudes to converge to the target distribution.

Our technique for designing an electric field for generating prescribed wavepackets in diatomic molecules can then be summarized in a five-step recipe:

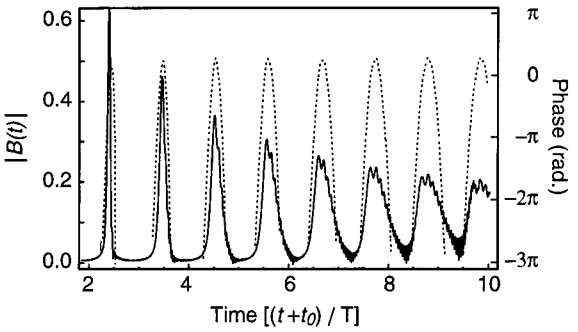

Figure 3. Amplitude (solid line) of the function $B(t)$ and its phase (dotted line) for a vibrational coherent state in the A state of K_2. Here, $\Delta = 0.01$.

1. Evaluate $B(t)$ from the target amplitudes.
2. Select a section of $B(t)$ by choosing an appropriate value for t_0.
3. Determine the driving field for the target using eq 13.
4. Check the field by numerically integrating eqs 2 and 3.
5. If population trapping occurs, go back to step 2, and choose the next longest impulse of $B(t)$.

The above recipe is the second major result of this paper. Together with eq 10, they describe a procedure for calculating the driving field that will generate a desired wavepacket in a diatomic molecule, and avoid population trapping in the ground electronic state.

To avoid many runs through this recipe, one should start with the longest section of $B(t)$ that is still constrained to one vibrational period. Of course, there is no guarantee a solution will be found for arbitrary states. Since $B(t)$ must have no structure, of significant amplitude, shorter than $\xi_{00}(t)$, solutions cannot be found for arbitrary states. For instance, a wavepacket consisting of half the population in the eigenstates at the extreme of the Franck−Condon transition will not be achieved with high fidelity. Of course, there is no guarantee that iterative methods will achieve high fidelity either.

V. Numerical Results

To illustrate the method of solution described in the previous sections, we now turn to the excitation of prescribed states in two molecules of different degrees of vibrational anharmonicity: the A state of K_2 (weakly anharmonic) and the B state of I_2 (strongly anharmonic).

In these examples, the weak-response regime is specified by a target depletion of $\Delta = 1\%$; that is, 1% of the electronic population of the initial state is transferred to the final state. For the strong-response case, this depletion is $\Delta = 99\%$.

A. Potassium Dimer. All the population was set to be initially in the lowest vibrational level of the X state of the potassium dimer. For simplicity, we ignored the dependence of the electronic dipole moment with internuclear distance, and assigned to it a value of 11.4 D—the value at the Franck−Condon region.[52] The frequencies ω_{ej} and the Franck−Condon factors for the X and A states were calculated from the potentials of ref 53.

We chose as test cases two prototypical localized states that exhibit both classical and quantum features.

The first of these test cases was a localized, vibrational quasi-coherent-state wavepacket centered at $\bar{\nu} = 10$ in the A state. Here, the target amplitudes were taken to be $b_j^{(T)} e^{-i\omega_{ej}\tau_0} = \{\Delta[\bar{\nu}^j \exp(-\bar{\nu})/j!]\}^{1/2}$ with $j = 0, 1, ..., M$ and $\tau_0 = 2T$. Figure 3 shows $B(t)$ for this target distribution—step 1 of our five-step recipe. We chose the impulse of $B(t)$ corresponding to $t_0 = -7.2T$—step 2. This is the longest section still constrained to about one vibrational period, thus a good candidate to avoid population trapping in the ground electronic state.

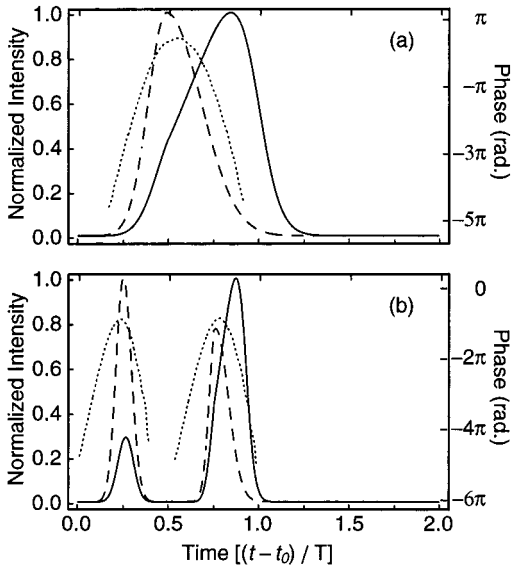

Figure 4. Driving fields for generating (a) a coherent state, and (b) a "cat" state in the A state of K_2. In both cases, the dashed line is the weak field intensity, the solid line is the strong field intensity, and the dotted line is the phase. The peak intensities, for the strong-response case, are (a) 3.6×10^9 W/cm^2 and (b) 7.6×10^9 W/cm^2. The weak fields are about 2-orders of magnitude lower in intensity than the strong fields. The target time is $\tau_0 = 2T$, and $T \approx 470$ fs.

The driving fields, determined from eq 13, are shown in Figure 4a for both small (1%) and large (99%) ground-state *target* depletion—step 3. A closer inspection of Figure 3 reveals ripples in $B(t)$ not seen in Figure 4a. This is because each section of $B(t)$ used in evaluating the corresponding driving fields was filtered to remove high-frequency components prior to being substituted in eq 13. As will be discussed next, not only did this filtering not alter the ability of the driving field to generate the wavepacket, but it also allows for temporal shapes that are more convenient to be reproduced in the laboratory. Such robustness to small changes in pulse shape has also been observed previously by others.[34]

Note that the shape of the field (although not the pulse energy) in the strong-response case is not radically different from that in the weak-response regime, and the differences make good physical sense. In the strong-response case, the dynamics are easily understood from the following argument: By the time the trailing edge of the pulse arrives at the system, the ground-state population is greatly reduced from its initial value, and there is consequently less absorption than at the leading edge of the pulse. Therefore, the pulse must be more intense at the trailing edge in order to be able to pump whatever population is left in the ground state up to the excited electronic state. Also noteworthy is the fact that the temporal phase of the driving field is exactly the same in both regimes of excitation. That is because the phase is determined only by the choice of target amplitudes, through $B(t)$, in eq 13.

The validity of these approximate solutions was tested by substituting the designed fields back into Schrödinger's equation (eqs 2 and 3) and numerically integrating without any further approximations to find the final state—step 4; we will refer to this as the "actual" state. Multiphoton excitation processes were not included in the simulations because the control field intensities were always less than 10^{10} W/cm^2, even in the regime of nearly total population transfer to the excited state. At these

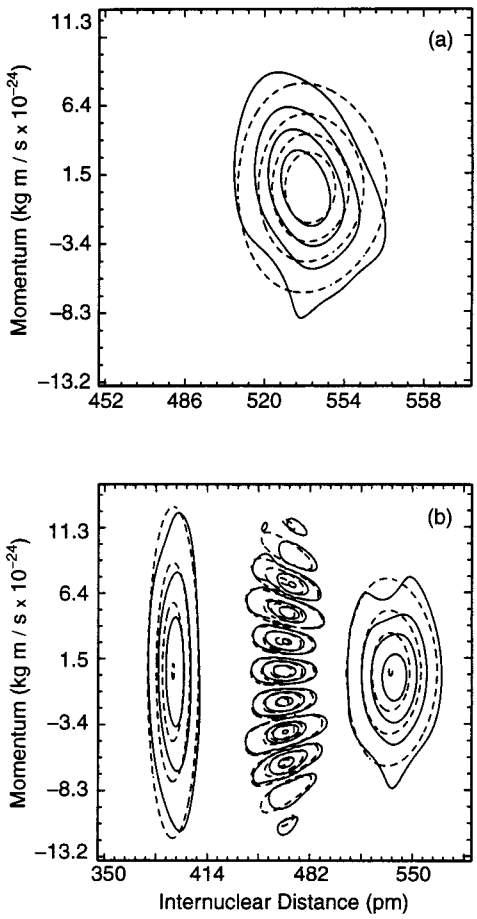

Figure 5. Phase-space representation of the target (dashed lines) and the "actual" (solid lines) for (a) a coherent state, and (b) a "cat" state in the A state of K_2, in the strong-response regime. Here, we plotted the Wigner function: $W(r,p) = \int_0^\infty dx\ \psi^*(r - x/2)\psi(r + x/2)\ e^{-isp/\hbar}$ where $\psi(r)$ is the wave function of either the target or "actual" states.

intensities, very little population (less than 0.2%) is transferred to higher excited states.[54] Figure 5a shows the target (dashed lines) and actual (solid lines) states in phase space for the strong-response case. One can see that excellent overlap between the two is obtained. In both weak- and strong-response regimes, the analytic prediction compares favorably with the full numerical results. To quantify the fidelity, we used a generalization of the achievement factor A,[34] defined by $A^2 = Tr(\hat{\rho}\hat{\rho}_T)/(Tr\ \hat{\rho}^2\ Tr\ \hat{\rho}_T^2)^{1/2}$, where $\hat{\rho}$ is the density operator associated with the final actual state in the upper manifold and $\hat{\rho}_T$ is that of the target state. Here, $A = 1$ when $\hat{\rho} = \hat{\rho}_T$, even for mixed states. In this article we deal only with pure states, so that our achievement factor is the same as that of Krause et al.[34]

We obtained an achievement of $A = 1.00$ in the weak-response regime and $A = 0.99$ in the strong-response regime, indicating that the target state was obtained with very high accuracy in both cases. The actual depletions accomplished were 1% (weak response) and 96% (strong response).

For our second test case, we used eq 13 to design a field that generates a Schrödinger "cat" state[1,55−57] in the excited electronic state. This state corresponds to a coherent superposition of two classically distinguishable quasi-coherent states: the nuclei are simultaneously localized at both inner and outer turning points of their trajectories. Here, $b_j^{(T)}e^{-i\omega_{ej}\tau_0} = \{\Delta[\bar{\nu}^j\ \exp(-\bar{\nu})/j!]\}^{1/2}$ $[(-1)^j + 1]$ and as before, $j = 0, 1, ..., M$; $\bar{\nu} = 10$; and $\tau_0 = 2T$. The field that generates such a distribution is shown in Figure 4b for both weak and strong excitation regimes (with $t_0 = -3.3$ T). As one would expect, two pulses are necessary to produce this state.[1,55−57] The second pulse arrives approximately a time T/2 after the first pulse and creates a second wavepacket, of identical configuration space structure to the first. This second wavepacket interferes with the first one, cancelling the population in the odd-numbered levels. Again, the differences between pulse shapes from the small to the large depletion case can be explained by the smaller absorption seen by the second pulse, and the rapid depletion of the ground state during each pulse. The difference in shape of the two pulses in the weak-response regime is due to the anharmonicity of the potential, meaning that the wavepacket changes shape as it propagates toward the outer turning point. Figure 5b shows the target (dashed lines) and actual (solid lines) states in phase space for the strong-response case. Again, very good overlap between the two is achieved. Here, $A = 1.00$ and actual depletion 1% in the weak-response case; and $A = 0.94$ and actual depletion 94% in the strong-response case.

Contrary to the first test case, the strong-response pulses for generating "cat" states do not have to be necessarily very long in order to avoid population trapping. That is because the boundary between the two regimes of excitation, weak and strong, is not a clear one. In the first case, a single pulse depletes the ground state by 96%, whereas in this second case, the first pulse depletes the ground state by less than 60%. It is very difficult to tell exactly when population trapping will become a problem; one has to go through the five steps of the recipe, until the appropriate driving field is found. Note, however, that the recipe involves only a single integration of Schrödinger's equation using a prescribed field (in order to determine the fidelity of the final state); a step which is found in all iterative methods as well.

B. Molecular Iodine. The B state of an iodine molecule is more anharmonic than the A state of a potassium molecule. Also, the Franck−Condon factors for transitions between the B state and the ground vibrational−electronic state are centered around the vibrational number $j = 30$, making the vibrational frequencies' spacing even more irregular. As a consequence, the electronic response function is wider than that for K_2 and its several impulses are more separated from one another in time. In this case, the driving field can actually be longer than a vibrational period without causing Rabi cycling between the X and B states.

For the numerical simulations, we again took the dipole moment to be independent of internuclear separation with a value of 1 D, at the Franck−Condon region.[58] Higher lying electronic states were not included in the simulations because the control field intensities were always less than 3.5×10^{12} W/cm^2.[34] The eigenfrequencies and the Franck−Condon factors for the X and B states were calculated from the potentials of ref 35.

As a target, we chose here the "molecular reflectron" wave packet.[33,34] Here, the excited wavepacket must reflect off the potential barrier, at the outer turning point, before it reaches its target shape: a localized Gaussian wavepacket with a small negative momentum. Figure 6 shows $B(t)$ for this target.

Say we first choose the narrow impulse of $B(t)$ corresponding to $t_0 = -1.6$T. This impulse should yield a smooth pulse that is well restricted to one vibrational period T. However, upon substitution into Schrödinger's equation, this driving pulse yields an achievement factor of $A = 0.64$ and a depletion of only 82%, in the strong-response regime, requiring us to take step 5 of our recipe. Here, the designed pulse is not long enough to completely avoid population trapping in the ground electronic

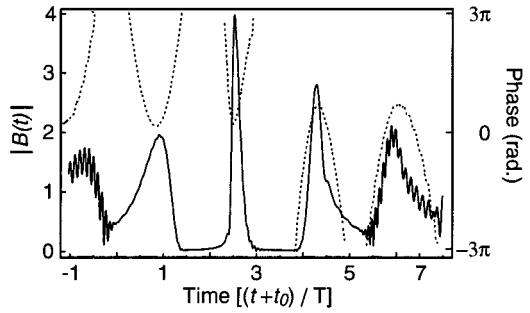

Figure 6. Amplitude (solid line) of the function $B(t)$, and its phase (dotted line) for the "molecular reflectron" in the B state of I_2. Here $\Delta = 0.99$, and the vibrational period is $T \approx 267$ fs.

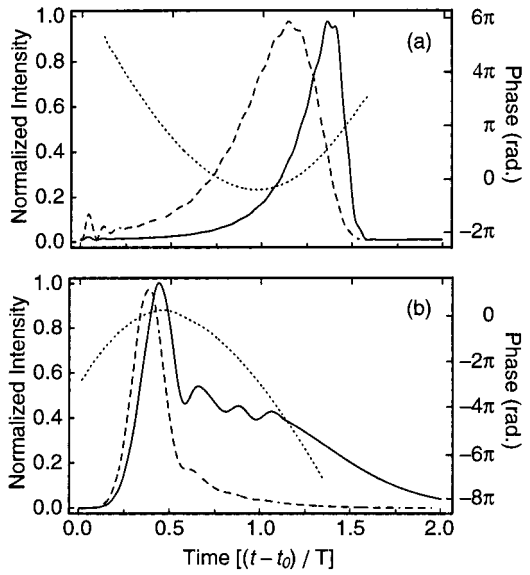

Figure 7. Driving field for creating the "molecular reflectron" in the weak (dashed line) and strong-response (solid line) regimes for (a) $t_0 = 0.25$T, and (b) $t_0 = -3.9$T. The peak intensities are (a) 3.3×10^{12} W/cm^2 and (b) 1.8×10^{12} W/cm^2 for the strong-response case. The weak fields are about 2 orders of magnitude lower in intensity than the strong fields. The target time is $\tau_0 = 2$T.

state. Figure 7a shows the weak and strong fields evaluated with the impulse of $B(t)$ corresponding to $t_0 = 0.25$T. The weak-response solution shown in Figure 7 is remarkably similar to that shown in Figure 6 of Krause et al.[33] The achievement factors we get from numerically integrating Schrödinger's equation are also quite similar: $A = 0.98$ in the weak-response case, and $A = 0.70$ in the strong-response case.[34] In the weak-response regime, the achievement factor is slightly lower than one might expect because the approximations of eqs 5 and 8 actually introduce a small time-dependent phase factor to $h(t)$. As for the low achievement of the strong-response solution, even though the field is long enough to avoid population trapping in the X state (the actual depletion is 96%, compared to the target of 99%), it is not very long compared to the electronic response function; eqs 5 and 8 are not very good approximations in this case. However, the section of $B(t)$ corresponding to $t_0 = -3.9$T yields a field of longer duration, resulting in a much better achievement factor: $A = 0.96$ with an actual depletion of 98%. Figure 7b shows the calculated driving pulses in both regimes of excitation, and Figure 8 shows the target and actual wavepackets for this case. As indicated by the high achievement factor, the overlap between the two (target and actual) is very good. Figure 9 shows the temporal dynamics of the ground vibrational states' amplitudes. One can see that the population in the levels $n \neq 0$ remains nearly unchanged (zero) throughout

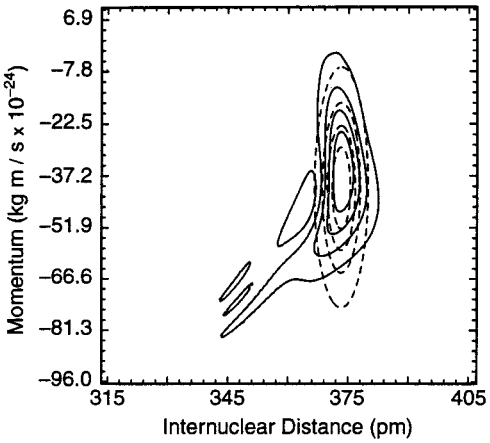

Figure 8. Phase-space (Wigner) representation of the target (dashed lines) and the "actual" (solid lines) "molecular reflectron", in the strong-response regime. The target state is represented by the wave function $\psi(r) = (2\pi\sigma)^{-1/4} \exp[-(x - \bar{x})^2/4\sigma + i(\bar{p}/\hbar)(x - \bar{x})]$, where $\bar{x} = 3.72$ Å, $\bar{p}^2/2m = 403$ cm^{-1}, $\bar{p} < 0$, and $\sigma = 4.6$ pm.

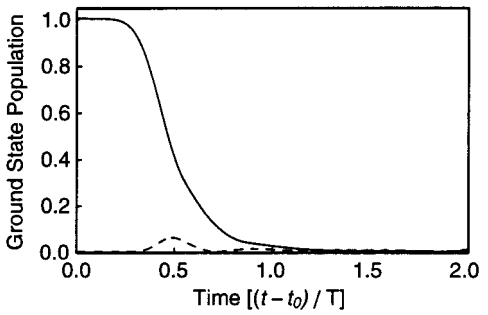

Figure 9. Ground-state depletion in the strong-response regime of I_2. The solid line is the population in level $n = 0$, and the dashed line is the total population in the other vibrational levels of the ground electronic state.

excitation, with at most 10% of the population going to the other vibrational levels at one time.

The pulses shown in Figure 7a,b have chirps of opposite signs. While the negatively chirped pulse of Figure 7a agrees with the OCT solution found by Krause et al.,[34] our results show that a positively chirped pulse can also focus a wavepacket. Even though the negatively chirped pulse yields a high degree of inversion, and an achievement factor adequate for an experiment,[34] the positive chirp solution is a better choice for a practical implementation. That is not just because it yields a higher achievement factor, but also because population inversion has been shown by Cao et al.[51] to be more robust (to small changes in the chirp) for positively chirped pulses.

VI. Conclusions

We have shown that the idea of restricting the driving force to a short enough duration that the discreteness of the system's level structure is not resolved leads to a great simplification of the nonlinear quantum control problem. In contrast to other approaches to quantum control, such as OCT, this restriction allows one to derive a simple approximate analytic solution for the driving field. This solution, evaluated directly from the target quantum state amplitudes in the excited manifold, holds even in the limit of large population transfer.

The two main approximations used in finding this analytic solution were that of a rapid electronic "response" function and the assumption of no population trapping occurring in the ground electronic state. These approximations were tested by substitut-

ing the driving field from eq 13 in eqs 2 and 3, which were then numerically integrated. As shown in Figures 5, 8, and 9, the approximations seem to hold well even in the strong regime. The key for these approximations to work is to chose among the many possible solutions ones for which the field is long compared to the response function, but at the same time shorter than one vibrational period. Obviously, this limits our technique to systems for which the duration of the electronic "response" function is significantly shorter than one vibrational period. Also, the family of wavepackets that are amenable to control using our scheme is restricted to those states that are accessible by a Franck−Condon transition from the initial ground vibronic state. These states must also have characteristic functions $B(t)$ whose impulses are longer than the electronic response function.

OCT is a more versatile technique that can be applied to a larger variety of problems and systems than the technique described here. For example, our technique would be very difficult to apply to the case in which one starts from an arbitrary population distribution in the ground electronic state. Because we chose to work in the Schrödinger representation, we are also limited to controlling only pure states. The main attraction of our technique is that by providing a simple, approximate analytic solution, it helps shed some light onto the physics behind the control of diatomic molecules in the strong-response regime.

Acknowledgment. L.d.A. acknowledges the financial support of CNPq (Conselho Nacional de Desenvolvimento Cient'fico e Tecnológico, Brazil). This work was supported in part by the NSF and the Army Research Office.

References and Notes

(1) Noel, M. W.; Stroud, Jr., C. R. *Phys. Rev. Lett.* **1996**, *77*, 1913.
(2) Weinacht, T. C.; Ahn, J.; Bucksbaum, P. H. *Nature* **1999**, *397*, 233.
(3) Dunn, T. J.; Sweetser, J. N.; Walmsley, I. A.; Radzewicz, C. *Phys. Rev. Lett.* **1993**, *70*, 3388.
(4) Vrakking, M. J. J.; Villeneuve, D. M.; Stolow, A. *Phys. Rev. A* **1996**, *54*, 37.
(5) Kohler, B.; Yakovlev, V. V.; Che, J.; Krause, J. L.; Messina, M.; Wilson, K. R.; Schwenter, N.; Whitnell, R. M.; Yan, Y. *Phys. Rev. Lett.* **1995**, *74*, 3360.
(6) Bardeen, C. J.; Jianwei, C.; Wilson, K. R.; Yakovlev, V. V.; Apkarian, V. A.; Martens, C. C.; Zadoyan, R.; Kohler, B.; Messina, M. *J. Chem. Phys.* **1997**, *106*, 8486.
(7) Bardeen, C. J.; Yakovlev, V. V.; Wilson, K. R.; Carpenter, S. D.; Weber, P. M.; Warren, W. S. *Chem. Phys. Lett.* **1997**, *280*, 151.
(8) Dunn, T. J.; Sweetser, J. N.; Walmsley, I. A.; Mukamel, S. *Phys. Rev. Lett.* **1995**, *74*, 884.
(9) Walmsley, I. A.; Waxer, L. *J. Phys. B* **1998**, *31*, 1825.
(10) Weinacht, T. C.; Ahn, J.; Bucksbaum, P. H. *Phys. Rev. Lett.* **1998**, *80*, 5506.
(11) Averbukh, I. S.; Shapiro, M.; Leichtle, C.; Schleich, W. P. *Phys. Rev. A* **1999**, *59*, 2163.
(12) Shapiro, M.; Brumer, P. *J. Chem. Phys.* **1986**, *84*, 4103.
(13) Shapiro, M.; Brumer, P. *J. Chem. Phys.* **1992**, *97*, 6259.
(14) Tannor, D. J.; Rice, S. A. *Adv. Chem. Phys.* **1988**, *70*, 441.
(15) Kosloff, R.; Rice, S. A.; Gaspard, P.; Tersigni, S.; Tannor, D. J. *Chem. Phys.* **1989**, *139*, 201.
(16) Shi, S.; Woody, A.; Rabitz, H. *J. Chem. Phys.* **1988**, *88*, 6870.
(17) Peirce, A. P.; Dahleh, M. A.; Rabitz, H. *Phys. Rev. A* **1988**, *37*, 4950.
(18) Gross, P.; Singh, H.; Rabitz, H.; Mease, K.; Huang, G. M. *Phys. Rev. A* **1993**, *47*, 4593.
(19) Warren, W. S.; Rabitz, H.; Mohammed, D. *Science* **1993**, *259*, 1581.
(20) Charron, E.; Giusti-Suzor, A.; Mies, F. H. *Phys. Rev. Lett.* **1993**, *71*, 692.
(21) Shnitman, A.; Sofer, I.; Golub, I.; Yogev, A.; Shapiro, M.; Chen, Z.; P., B. *Phys. Rev. Lett.* **1996**, *76*, 2886.
(22) Larsen, J. J.; Wedt-Larsen, I.; Stapelfeldt, H. *Phys. Rev. Lett.* **1999**, *83*, 1123.
(23) Chen, Z. D.; Shapiro, M.; Brumer, P. *J. Chem. Phys.* **1993**, *98*, 6843.
(24) Heberle, A. P.; Baumberg, J. J.; Kohler, K. *Phys. Rev. Lett.* **1995**, *75*, 2598.
(25) Dupont, E.; Corkum, P. B.; Liu, H. C.; Buchanan, M.; Wasilewski, Z. R. *Phys. Rev. Lett.* **1995**, *74*, 3596.
(26) I., B.; Planken, P. C. *J. Opt. Soc. Am. B* **1994**, *11*, 2457.
(27) Krause, J. L.; Shapiro, M.; Brumer, P. *J. Chem. Phys.* **1990**, *92*, 1126.
(28) Zare, R. N. *Science* **1998**, *279*, 1875.
(29) Manz, J.; Sundermann, K.; de Vivie-Riedle, R. *Chem. Phys. Lett.* **1998**, *290*, 415.
(30) Korolkov, M. V.; Paramonov, G. K.; Schimdt, B. *J. Chem. Phys.* **1996**, *105*, 1862.
(31) Korolkov, M. V.; Manz, J.; Paramonov, G. K. *Chem. Phys.* **1997**, *217*, 341.
(32) Manz, J.; Paramonov, G. K. *J. Phys. Chem.* **1993**, *97*, 12625.
(33) Krause, J. L.; Whitnell, R. M.; Wilson, K. R.; YiJing, Y.; Mukamel, S. *J. Chem. Phys.* **1993**, *99*, 6562.
(34) Krause, J. L.; Messina, M.; Yan, Y.; Wilson, K. R. *J. Phys. Chem.* **1995**, *99*, 13736.
(35) Che, J.; Krause, J. L.; Messina, M.; Wilson, K. R.; Yan, Y. *J. Phys. Chem.* **1995**, *99*, 14949.
(36) Averbukh, I. S.; Shapiro, M. *Phys. Rev. A* **1993**, *47*, 5086.
(37) Yan, Y. J.; Che, J. W.; Krause, J. L. *Chem. Phys.* **1997**, *217*, 297.
(38) Lozovoy, V. V.; Antipin, S. A.; Gostev, F. E.; Titov, A. A.; Tovbin, D. G.; Sarkisov, O. M.; Umanskii, S. Y. *Chem. Phys. Lett.* **1998**, *284*, 221.
(39) Bardeen, C. J.; Che, J. W.; Wilson, K. R.; Yakovlev, V. V.; Cong, P. J.; Kohler, B.; Krause, J. L.; Messina, M. *J. Phys. Chem. A* **1997**, *101*, 3815.
(40) Che, J. W.; Messina, M.; Wilson, K. R.; Apkarian, V. A.; Li, Z.; Martens, C. C.; Zadoyan, R.; Yan, Y. J. *J. Phys. Chem.* **1997**, *100*, 7873.
(41) Shen, L.; Shi, S.; Rabitz, H. *J. Phys. Chem.* **1993**, *97*, 12114.
(42) Kim, K. G.; Girardeau, M. D. *Phys. Rev. A* **1995**, *52*, 891.
(43) Zhu, W.; Rabitz, H. *J. Chem. Phys.* **1999**, *110*, 7142.
(44) de Araujo, L. E. E.; Walmsley, I. A.; Stroud, Jr., C. R. *Phys. Rev. Lett.* **1998**, *81*, 955.
(45) Suominen, K. A.; Garraway, B. M.; Stenholm, S. *Phys. Rev. A* **1992**, *45*, 3060.
(46) Morse, P.; Feshbach, H. *Methods of Theoretical Physics*; McGraw-Hill: New York, 1953.
(47) Ruhman, S.; Joly, A. G.; Nelson, K. A. *J. Chem. Phys.* **1987**, *86*, 6563.
(48) Yong-xin, Y.; Gamble, Jr., E. B.; Nelson, K. A. *J. Chem. Phys.* **1985**, *83*, 5391.
(49) Parker, J.; Stroud, Jr., C. R. *Phys. Rev. A* **1990**, *41*, 1602.
(50) Dubrovskii, Y. V.; Ivanov, M. Y.; Fedorov, M. V. *Laser Phys.* **1992**, *2*, 288.
(51) Cao, J.; Bardeen, C. J.; Wilson, K. R. *Phys. Rev. Lett.* **1998**, *80*, 1406.
(52) de Vivie-Riedle, R.; Kobe, K.; Meyer, W.; Reischl, B.; Rutz, S.; Schreiber, E.; Woste, L. *J. Phys. Chem.* **1996**, *100*, 7789.
(53) Lyra, A. M.; Luh, W. T.; Li, L.; Wang, H.; Stwalley, W. C. *J. Chem. Phys.* **1990**, *92*, 43.
(54) de Vivie-Riedle, R.; Reischl, B.; Rutz, S.; Schreiber, E. *J. Phys. Chem.* **1995**, *99*, 16829.
(55) Walmsley, I. A.; Raymer, M. G. *Phys. Rev. A* **1995**, *52*, 681.
(56) Janszky, J.; Vinogradov, A.; Kobayashi, T.; Kis, Z. *Phys. Rev. A* **1994**, *50*, 1777.
(57) Scherer, N.; Carlson, R.; Matro, A.; Du, M.; Ruggiero, A.J.; Romero-Rochin, V.; Cina, J.; Fleming, G.; Rice, S. *J. Chem. Phys.* **1991**, *95*, 1487.
(58) Tellinghuisen, J. *J. Chem. Phys.* **1982**, *76*, 4736.